Science Bulletin 64 (2019) 26–35

Contents lists available at ScienceDirect

Science Bulletin

journal homepage: www.elsevier.com/locate/scib

Article

Physical and toxicological profiles of human IAPP amyloids and plaques

Aleksandr Kakinen [a,1,*], Yunxiang Sun [b,1], Ibrahim Javed [a,c], Ava Faridi [a], Emily H. Pilkington [a], Pouya Faridi [d], Anthony W. Purcell [d], Ruhong Zhou [e,f], Feng Ding [b], Sijie Lin [c], Pu Chun Ke [a,*], Thomas P. Davis [a,*]

[a] ARC Centre of Excellence in Convergent Bio-Nano Science and Technology, Monash Institute of Pharmaceutical Sciences, Monash University, VIC 3052, Australia
[b] Department of Physics and Astronomy, Clemson University, Clemson, SC 29634, USA
[c] College of Environmental Science and Engineering, Shanghai Institute of Pollution Control and Ecological Security, Biomedical Multidisciplinary Innovation Research Institute, Shanghai East Hospital, Tongji University, Shanghai 200092, China
[d] Infection and Immunity Program & Department of Biochemistry and Molecular Biology, Biomedicine Discovery Institute, Monash University, Clayton, Victoria 3800, Australia
[e] IBM Thomas J. Watson Research Center, Yorktown Heights, NY 10598, USA
[f] Department of Chemistry, Columbia University, New York, NY 10027, USA

ARTICLE INFO

Article history:
Received 9 August 2018
Received in revised form 14 November 2018
Accepted 19 November 2018
Available online 22 November 2018

Keywords:
IAPP
Amyloid
Plaque
Self assembly
Toxicity

ABSTRACT

Although much has been learned about the fibrillization kinetics, structure and toxicity of amyloid proteins, the properties of amyloid fibrils beyond the saturation phase are often perceived as chemically and biologically inert, despite evidence suggesting otherwise. To fill this knowledge gap, we examined the physical and biological characteristics of human islet amyloid polypeptide (IAPP) fibrils that were aged up to two months. Not only did aging decrease the toxicity of IAPP fibrils, but the fibrils also sequestered fresh IAPP and suppressed their toxicity in an embryonic zebrafish model. The mechanical properties of IAPP fibrils in different aging stages were probed by atomic force microscopy and sonication, which displayed comparable stiffness but age-dependent fragmentation, followed by self-assembly of such fragments into the largest lamellar amyloid structures reported to date. The dynamic structural and toxicity profiles of amyloid fibrils and plaques suggest that they play active, long-term roles in cell degeneration and may be a therapeutic target for amyloid diseases.

1. Introduction

Protein misfolding and aggregation, regardless of their sequence and culprit origin, is a ubiquitous phenomenon in neurodegenerative disorders and type 2 diabetes mellitus (T2DM), characterized by the kinetic processes of nucleation, elongation and saturation towards a cross-β architecture for nearly all amyloid proteins [1–4]. It has now been established that the oligomeric species formed on or off pathway to amyloid fibrils elicit toxicity [5–7], while the amyloid hypothesis [8] has become much less influential of late, despite reports of active physiological behaviors of amyloid fibrils [9,10].

Experiments with transgenic mice revealed that injection of exogenous beta-amyloid (Aβ) aggregates from various sources produced different distributions and quantities of plaques [11–13]. Similarly, $A\beta_{40}$ fibrils seeded by amyloids extracted from the brain tissues of patients developed miscellaneous polymorphs, manifesting significantly different clinical histories [14]. From the "seeding" experiments, i.e., adding β sheet-rich amyloid fragments to induce re-growth of "seeds" into long fibrils, it has been demonstrated that mesoscopic features such as fibril width and twisting periodicity can pass on from seeds to freshly-grown fibrils [15,16]. However, it remains largely unknown as how the physical properties of amyloids may evolve beyond the saturation phase—usually less than 48 h as in a thioflavin T (ThT) or Congo red kinetic assay—and how such changing physical properties may translate to biological effects.

Human islet amyloid polypeptide (IAPP) is a 37-residue peptide co-synthesized and co-stored with insulin in pancreatic β-cells [17]. IAPP in the monomeric form is responsible for glycemic control in cooperation with insulin. Aberrant environmental conditions, such as deficiencies in insulin or metals (e.g., zinc), association of IAPP with cell membranes, or disruption to zinc-coordinated IAPP and C-peptide complexation, may trigger changes in IAPP conformation and subsequent aggregation [4,18–21], leading to the onset of oxidative and inflammatory stress, β-cell death and T2DM, a metabolic disease and a global

* Corresponding authors.
E-mail addresses: aleksandr.kakinen@monash.edu (A. Kakinen), pu-chun.ke@monash.edu (P.C. Ke), thomas.p.davis@monash.edu (T.P. Davis).
[1] These authors contributed equally to this work.

https://doi.org/10.1016/j.scib.2018.11.012
2095-9273/

epidemic. Similarly to what is known for other amyloid proteins such as Aβ and alpha-synuclein, IAPP oligomers have been implicated as the most toxic [22], while IAPP fibrils have been found to perturb membrane fluidity through lipid extraction [4,23,24]. To fill a knowledge gap in amyloidosis, here we examined in detail the structural and toxicity profiles of IAPP amyloid fibrils beyond the conventional saturation phase. Our findings revealed the evolving physical and biological properties of amyloid fibrils and plaques aged up to 2 months—some of which unexpected—that warrant consideration for the development of therapeutic strategies against amyloid diseases.

2. Materials and methods

2.1. Materials

IAPP (37-residue sequence: KCNTATCATQRLANFLVHSSNN FGAILSSTNVGSNTY; disulfide bridge: 2–7; M_W: 3906; >95% pure by high-performance liquid chromatography (HPLC)) was obtained as lyophilized powder from AnaSpec. The IAPP peptide was reconstituted overnight in 100% hexafluoro-2-isopropanol (HFIP) to dissolve all preformed aggregates (HPLC and mass spectroscopy characterizations of IAPP refer to Figs. S1 and S2 online). Then the solution was freeze-dried and a stock solution was prepared in water at a concentration of 200 μmol/L (IAPP readily fibrillates at μmol/L concentrations in vitro) and was allowed to fibrillate at room temperature for 2 h, 1 day, 1 week or 2 months to acquire amyloids of different ages. It should be pointed out that amyloid proteins may aggregate orders of magnitude slower in vivo than in test tubes, due to the presence of chaperones, metal ions and cell membranes [4]. The selected time points of 2 h, 1 day, 1 week, and 2 months in the present study intend to represent the rich heterogeneity of amyloid protein aggregates, their coexistence and evolution. This design does not eliminate monomeric and oligomeric/protofibrillar species that may coexist with fibrillar IAPP, but rather reports on the changing physical and biological properties of IAPP over time. The amyloid solutions were premixed before use to homogenize fibril suspensions. All solutions were prepared in 2 mL glass tubes using ultrapure Milli-Q water (18.2 MΩ cm; Millipore Corporation, USA).

2.2. Transmission electron microscopy

Sonicated and un-sonicated IAPP amyloid fibrils of different ages were examined using transmission electron microscopy (TEM). For this a 5 μL of amyloid-containing solution was pipetted onto glow discharged (15 s) copper grids (400 mesh; ProSciTech), followed by 1 min of adsorption. Excess samples were then drawn off using filter paper and the grids were washed by Milli-Q water with the excess drawn off. The grids were stained for 30 s with a drop of 1% uranyl acetate, then the excess stain was drawn off and the grid was air dried. Imaging was performed by a Tecnai G2 F20 transmission electron microscope (FEI, Eindhoven, The Netherlands) operated at a voltage of 200 kV. Images were recorded using a Gatan UltraScan 1000 (2 k × 2 k) CCD camera (Gatan, California, USA) and Gatan Microscopy Suite control software.

2.3. Fourier transform infrared spectroscopy

FTIR spectra were obtained using a Shimadzu IRTracer-100 spectrophotometer. For this 5 μL of 25 μmol/L IAPP were placed on a sample holder, air dried and the spectra were acquired between 1000 and 4,000 cm^{-1} at 20 °C with resolution of 4 cm^{-1}. The spectrum of a blank was acquired and subtracted from the sample spectra.

2.4. Circular dichroism spectroscopy

Circular dichroism (CD) spectra of IAPP amyloids (25 μmol/L) of different ages were obtained for the wavelength range of 190–260 nm with a 1 nm step size at room temperature. The CD spectra were taken using a Chirascan Plus qCD instrument (Applied Photophysics). The measurement was performed in triplicate and average spectra of 3 measurements were analyzed.

2.5. Atomic force microscopy

A droplet of 20 μL of IAPP amyloid sample solution (25 μmol/L) was deposited and incubated for 2 min on freshly cleaved mica, rinsed with Milli-Q water, and dried with air. Nanomechanical characterization (QNM-AFM) of IAPP amyloids was performed using a Cypher AFM (Asylum Research) operating in the AM-FM viscoelastic mapping mode in air at a scan rate of 1 Hz. AFM cantilevers (Olympus) were calibrated on the calibration samples prior to measurements. Selected areas with individual fibrils were analyzed for their nanomechanical characterizations.

2.6. Ultrasonication of amyloid fibrils

Aged amyloid fibrils were sonicated using a Vibra-Cell™ Ultrasonic VCX 750 sonicator equipped with a 3 mm microtip. Sonication was performed in 1.5 mL tubes (Eppendorf EG, Germany) cooled in ice bath with a sample volume of 0.5 mL each. Sonication of 1, 2 and 4 min at 20% of the maximum output power of the sonicator was applied.

2.7. Blue-native PAGE and gel analysis

IAPP amyloid fibrils (100 μmol/L) were incubated with human serum albumin (HSA, 100 μmol/L) for 4 h in Milli-Q water and then 15 μL were transferred to 4%–15% gel (Mini-Protean TGX) and blue-native polyacrylamide gel electrophoresis (PAGE) was performed using Tris/Glycine buffer at pH 8.3. For protein binding capacity a densitometry of protein bands was performed using the standard methods of ImageJ [25]. The experiment was performed and analyzed in duplicate.

2.8. Thioflavin T assay

IAPP fibrillization in the presence of mature amyloids or seeds from sonicated fibrils was analyzed by a thioflavin T (ThT) assay. For this 25 mmol/L ThT dye, 25 μmol/L of IAPP monomers and 2.5 μmol/L of IAPP fibrils/seeds were mixed and ThT fluorescence (read from bottom) were recorded every 10 min over 24 h at 25 °C, using an EnSpire Multimode Plate Reader (PerkinElmer; excitation/emission: 440 nm/485 nm) and a 96-well plate (Costar black/clear bottom). The ThT kinetic assay was performed in triplicate and average spectra of 3 measurements were analyzed and presented.

2.9. Viability in vitro

Pancreatic βTC6 cells (ATCC) were seeded in complete media (DMEM, 15% fetal bovine serum or FBS) at a density of 5×10^5 cells/well in a 96-well black/clear bottom plate (Costar), precoated with poly-D-lysine to promote cell adhesion. Prior to the experiment, media was refreshed. Fresh IAPP and IAPP amyloids (final concentration: 25 μmol/L) were added to wells containing complete media with 1 μmol/L propidium iodide (PI, AnaSpec; excitation/emission: 535 nm/617 nm) and read on an Operetta High-Content Imaging system (PerkinElmer) with a built-in live cell chamber (37 °C, 5% CO_2) every hour for 24 h. The percentage

of PI-positive cells, as indicative of cell death, was calculated as the number of stained nuclei relative to the total cell count determined by the built-in bright-field mapping function of Harmony High-Content Imaging and Analysis software (PerkinElmer), presented as the average of 5 reads/well. The measurement was performed in triplicate and average results were presented.

2.10. Reactive oxygen species (ROS) assay

ROS detection was performed using a DCFH-DA cellular ROS detection kit (OxiSelect Intracellular ROS Assay Kit, Cell Biolabs). Pancreatic βTC6 beta cells were stained with DCFH-DA for 60 min and subsequently treated with fresh (0 h), 2 h pre-incubated IAPP, 1 day old, 1 week old and 2 months old IAPP amyloids (50 μmol/L final concentration) for 4 h. ROS levels were then measured indirectly by the oxidation of non-fluorescent DCFH-DA to fluorescent DCF using a Multimode Plate Reader (EnSpire, PerkinElmer) at 480 nm of excitation and 530 nm of emission wavelength. The assay was performed with 96-well plates (Corning) for 4×10^5 cells/well at 37 °C. One-way ANOVA (Dunnett's multiple comparisons test) was used for statistical analysis.

2.11. Embryonic zebrafish toxicity assay

The AB wild-type zebrafish (*Danio rerio*) was housed in a fish breeding circulatory system (Haisheng, Shanghai, China) operated at (28 ± 0.5) °C on a 14 h:10 h light/dark cycle. Embryos were collected by adult spawning triggered upon first light in the morning. Injection mixtures were prepared by mixing fresh IAPP (12 μmol/L final concentration) with different aged IAPP fibrils (12 or 1.2 μmol/L final concentration for 1:1 or 10:1 by volume ratio). The mixtures were prepared immediately before microinjections into zebrafish embryos. A 15 μmol/L of ThT dye was included in the IAPP injection mixtures to enable imaging of fibrillated IAPP within the embryos. Microinjections were performed with a pneumatic microinjection system (PV830 Pneumatic Picopump, WPI) and the injection volume was set at 5 nL, under an injection pressure of 20 psi. Holtfreter's buffer [26] was used to prepare all the solutions for microinjections. Embryos were incubated at (28 ± 0.5) °C in Holtfreter's buffer in a 96-well microplate and imaged at 0, 6 and 12 h to study interactions of IAPP species with the embryos. The development and hatching of the embryos were then monitored for 3 days. Imaging was performed under the green fluorescence channel (GFP) of a fluorescence microscope (EVOS FL Auto, Life Technologies). A 5 nL of 15 μmol/L ThT in Holtfreter's buffer was injected in control embryos. The toxicity of IAPP against zebrafish embryos was presented as percentage of embryos died during the 3 days of development. The assay was performed in triplicate, with 3 groups ($n = 20$) of embryos per sample condition.

2.12. IAPP statistical analysis

IAPP fibril analysis was conducted with software FiberApp [27] to determine the contour length of IAPP fibrils. The FiberApp open source code was developed based on statistical polymer physics and enables structural analysis at the single molecular level of high-resolution imaging of fiber-like, filamentous, and macromolecular objects. The contour length corresponds to the end-to-end length of a polymer along its contour. The thickness of the fibrils was analyzed by ImageJ (National Institutes of Health).

2.13. Computational method

The initial atomic coordinates of IAPP protofibrils were set up according to the solid-state NMR study by the Tycko group [28]. In this model, IAPP peptides formed an in-registered parallel β-strand-turn-β-strand structure. The β-strand regions were located at the N-terminus (residues Lys1-Val17) and C-terminus (Ser28-Tyr37), linked by a turn spanning residues His18-Leu27 [28]. The protofibril unit at the fibril cross-section was composited by two IAPP peptides (Fig. S3a online). Each protofibril was built by parallel stacking of adjacent peptides with a separation of ~4.8 Å and a left-handed rotation of ~1.8° along the fibril axis (*z*-direction in Fig. S3a online). Two 10 nm protofibril fragments of 20×2 peptides were used to study their lateral association leading to a fibril fragment of 20×4 peptides at the atomic level. The association configurations of two protofibrils were systematically sampled by adjusting their inter-protofibril displacements along the *x*- and *y*-directions as shown in Fig. S3a (online). The strands were kept parallel to each other in the cross-section plane since relative rotations of the two protofibril fragments would decrease their contact surface area. Relative shifting from 0 to 3.99 nm with a step of 0.33 nm in the *x* direction and from 3.5 to 6.0 nm with a step of 0.1 nm in the *y* direction (Fig. S3a online) resulted in 382 total inter-protofibril arrangements. For each conformation, 20 independent Monte Carlo-based annealing simulations were performed to sample the side-chain packing along the inter-protofibril interface. The Monte Carlo-based annealing simulations were performed using MedusaDork [29,30] with the backbone fixed and sidechain of interface residues routable to sample the lowest energy state according to Metropolis criterion. The simulation temperature was gradually reduced from 10 kcal/mol k_B till the acceptance rate was below a pre-defined threshold [31]. With averaged total energy of each complex from 20 independent simulations, the corresponding binding energy was estimated as the energy difference between the two-protofibril complexes and the two separated protofibrils. The Medusa all-atom implicit solvent force field was used in the energy calculation [32,33].

3. Results and discussion

3.1. IAPP aggregation and structural properties

Upon incubation in water, freshly formed amyloids (up to a week) appeared as thin long fibrils (Fig. 1b and c). However, amyloids become more interconnected upon aging, as indicated by the formation of plaques (Fig. 1d). Circular dichroism (CD) spectroscopy (Fig. 1e) and Fourier transform infrared spectroscopy (FTIR) (Fig. 1f) revealed that IAPP amyloids underwent structural transformations over time, leading to increased β-sheets and turns. Moreover, both long fibrils and small aggregates were detected by TEM (Fig. 1a–c) for IAPP aged from several hours up to one week. While oligomers are often considered as on-pathway aggregation intermediates and gradually disappear during fibril formation [34], literature also suggests that the formation of oligomers may occur parallel to the pathway of protein amyloid aggregation, yielding stable and toxic aggregates of various morphologies and sizes [35–38]. In the present study, we noticed the occurrence of oligomeric aggregates of (58 ± 38) nm, which coexisted with mature amyloids in solution up to one week.

3.2. IAPP amyloid-physical properties

3.2.1. Nanomechanical properties, probed by AFM

We applied quantitative nanoscale mechanical atomic force microscopy (QNM-AFM) to identify the effect of amyloid aging on the structural features and their associated nanomechanical properties of IAPP fibrils (Fig. 2). Surprisingly, the variations of measured elastic modulus (Young's modulus, *E*) for different aged amyloids were minor within the experimental error. Namely, the

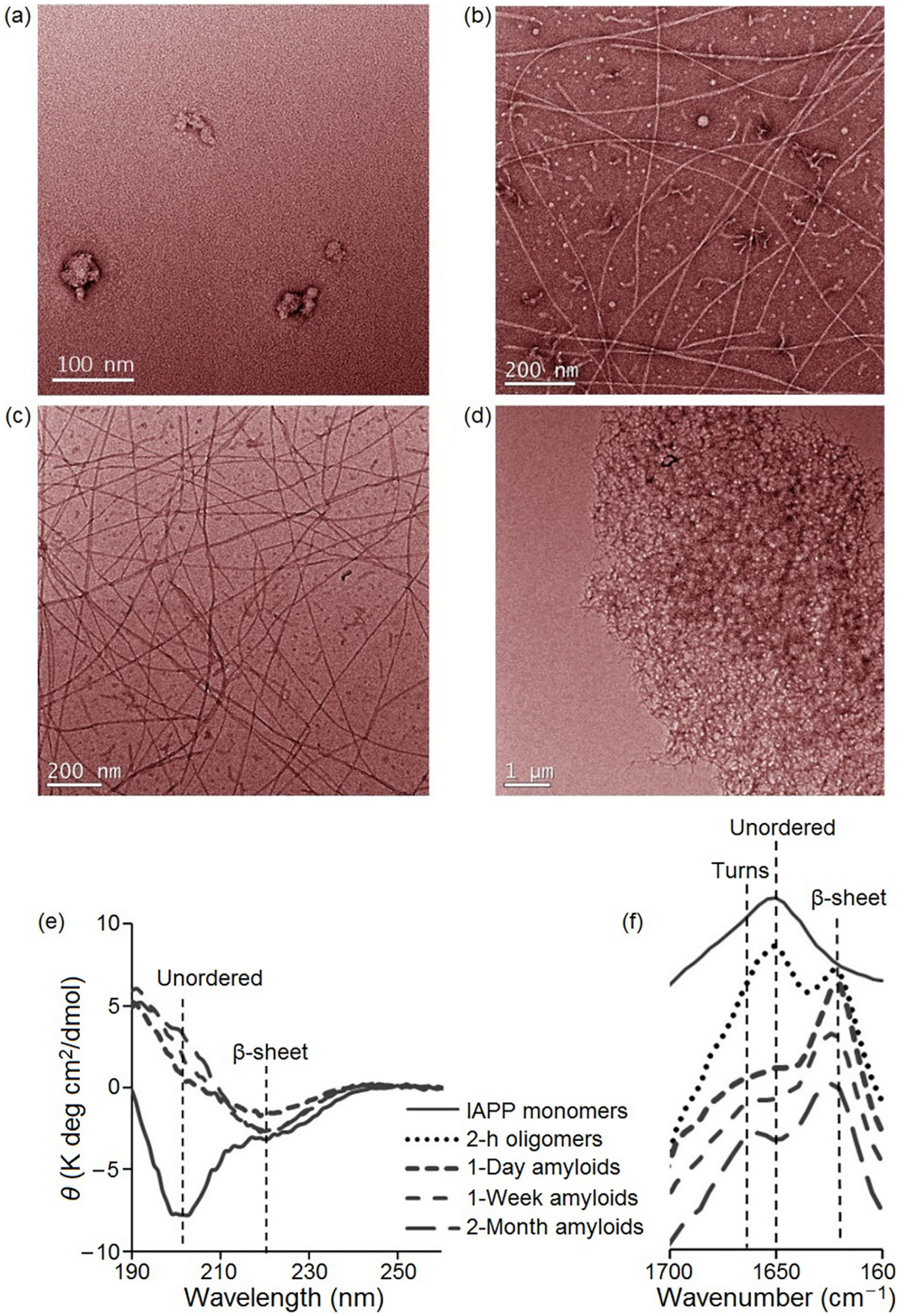

Fig. 1. (Color online) Evolving morphological and structural properties of IAPP over time. Negative-stain TEM of IAPP after 2 h (a), 1 day (b), 1 week (c), and 2 months (d) of fibrillization. (e) CD analysis of IAPP monomers, 1-day, 1-week and 2-month old IAPP amyloids. (f) FTIR amide I spectra showing increased β-sheets (~1,622 cm^{-1}) and β-turns (~1,664 cm^{-1}) with aging of IAPP amyloids. The amide I (1,600–1,700 cm^{-1}) band is due to C=O stretching vibrations of the peptide bonds, which are modulated by the secondary structure (unordered, β-sheets, etc.).

Young's moduli for 1-day, 1-week and 2-month old fibrils were (3.3 ± 0.3) GPa (Fig. 2c), (3.5 ± 0.4) GPa (Fig. 2f) and (3.5 ± 0.3) GPa (Fig. 2i), respectively, comparable to that of Aβ and Tau fibrils [39].

3.2.2. Physicochemical and self-assembly properties, probed by sonication

Sonication has been used for examining fibril formation [40,41], obtaining "seeds" from amyloids [42–44], and restoring memory in

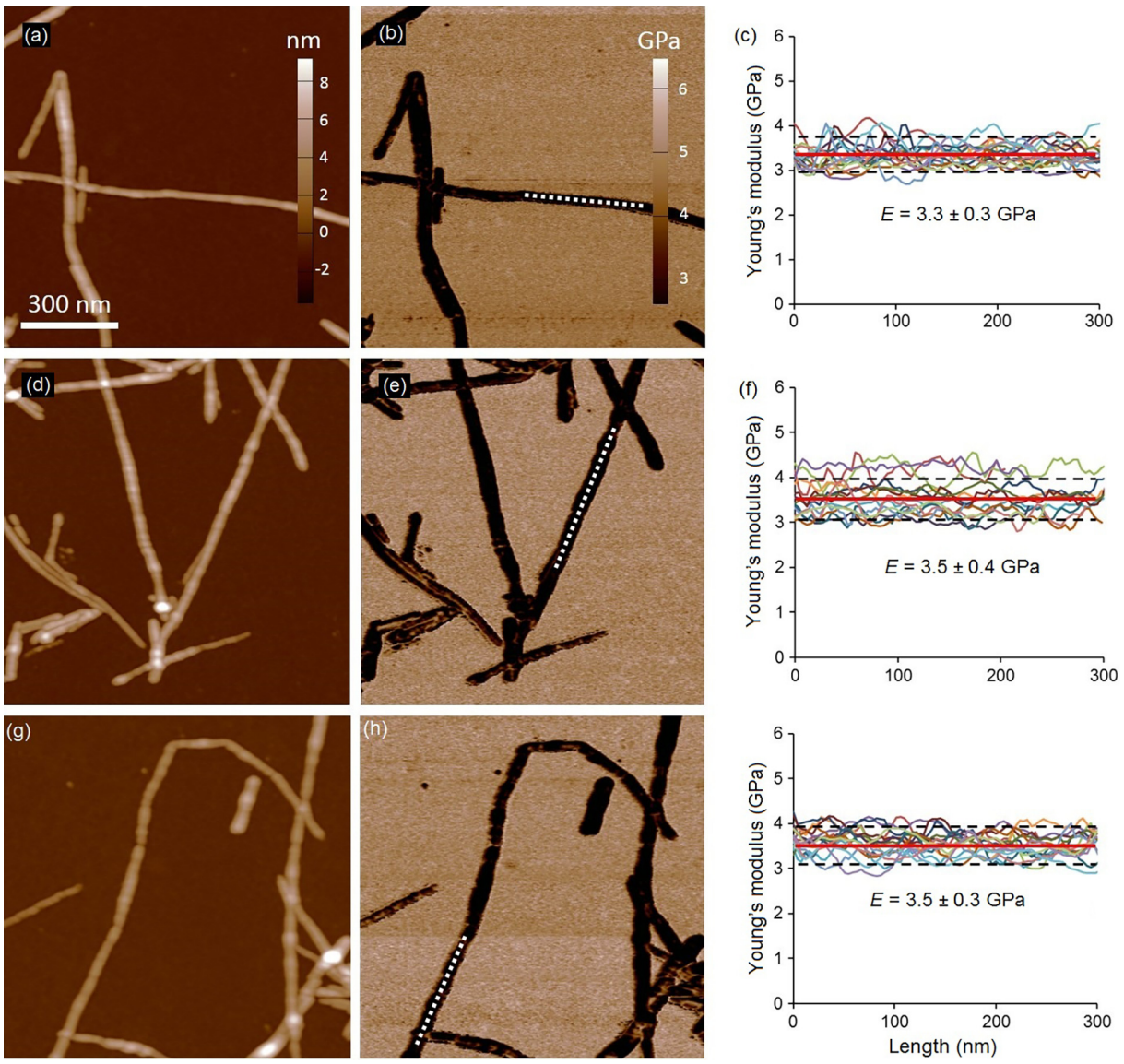

Fig. 2. Evolving mechanical properties of IAPP over time. Quantitative nanoscale mechanical AFM of 1-day (a)–(c), 1-week (d)–(f) and 2-month (g)–(i) old IAPP amyloid fibrils. AFM height images (a), (d), (g) and Young's modulus images (b), (e), (h) of 1-day, 1-week and 2-month old IAPP amyloids, respectively. Dashed white lines represent areas taken for the analysis. Young's modulus profiles of 1-day (c), 1-week (f) and 2-month (i) old IAPP fibrils (15 fibrils analyzed for each type).

an Alzheimer's disease mouse model by clearing amyloids via the lysosomes of energized microglia [45]. Here we applied sonication to probe the physical properties of fresh and aged amyloids (Fig. 3). We used a probe-sonicator operated at 20% of its maximum output power and applied that to a fixed volume of 0.5 mL for all samples. To determine the sonication power applied to a sample, the term specific energy (E_{spec}) is used [46,47]. E_{spec} (kJ/m^3) is a function of the delivered acoustic power P (W) (the energy consumed for breaking amyloids but also led to thermal loss), time t (s) and sample volume V (m^3) with the following relation: $E_{spec} = P \times t/V$. Thus, with a constant sample volume and a constant device output power, E_{spec} is proportional to sonication time only.

Despite the minor variations of elasticity among fibrils of different ages (Fig. 2), sonication revealed substantial differences in the capacity of fragmentation and re-assembly amongst the IAPP fibril species. Specifically, ultrasound was able to break the 1-day and 1-week old fibrils into relatively long fragments ((310.8 ± 217.3) nm and (193.4 ± 127.7) nm, respectively) (Fig. 3a and b), while cutting 2-month old IAPP amyloids into much smaller pieces (Fig. 3d–f). By increasing the duration of sonication we observed decreases in contour length for fragmented 2-month old amyloids, from (75.0 ± 33.5) nm after 1 min of sonication down to (23.2 ± 6.2) nm for 2 min of sonication and (14.8 ± 3.9) nm for 4 min of sonication (Fig. 4h). In comparison, the contour length of untreated IAPP amyloids can be up to 20 μm [48].

An empirical relationship was established between the ratio of fragment length to width ((6 ± 2) nm by TEM) (L/W ratio) and post-sonication fibril formation in solution (Fig. 3h). At high L/W ratios (>32) the sonicated fragments did not display the tendency of re-alignment but assumed disordered associations (Fig. 3a). At L/W ratios between 32 (Fig. 3b) and 12 (Fig. 3d) amyloid fragments exhibited an ability of re-aligning sideways into long fibrils, likely through hydrophobic interaction, π-stacking and H-bonding (Fig. 3c). At lower L/W ratios (<12) short amyloid fragments re-assembled into giant "stripe"-like 2D topologies surpassing 1 μm in width at times (Figs. 3e, f and S4 (online)). These, to our knowledge, are the largest lamellar structures observed for any amyloid proteins [49]. Furthermore, at L/W ratio = 4 the formed "stripe"-

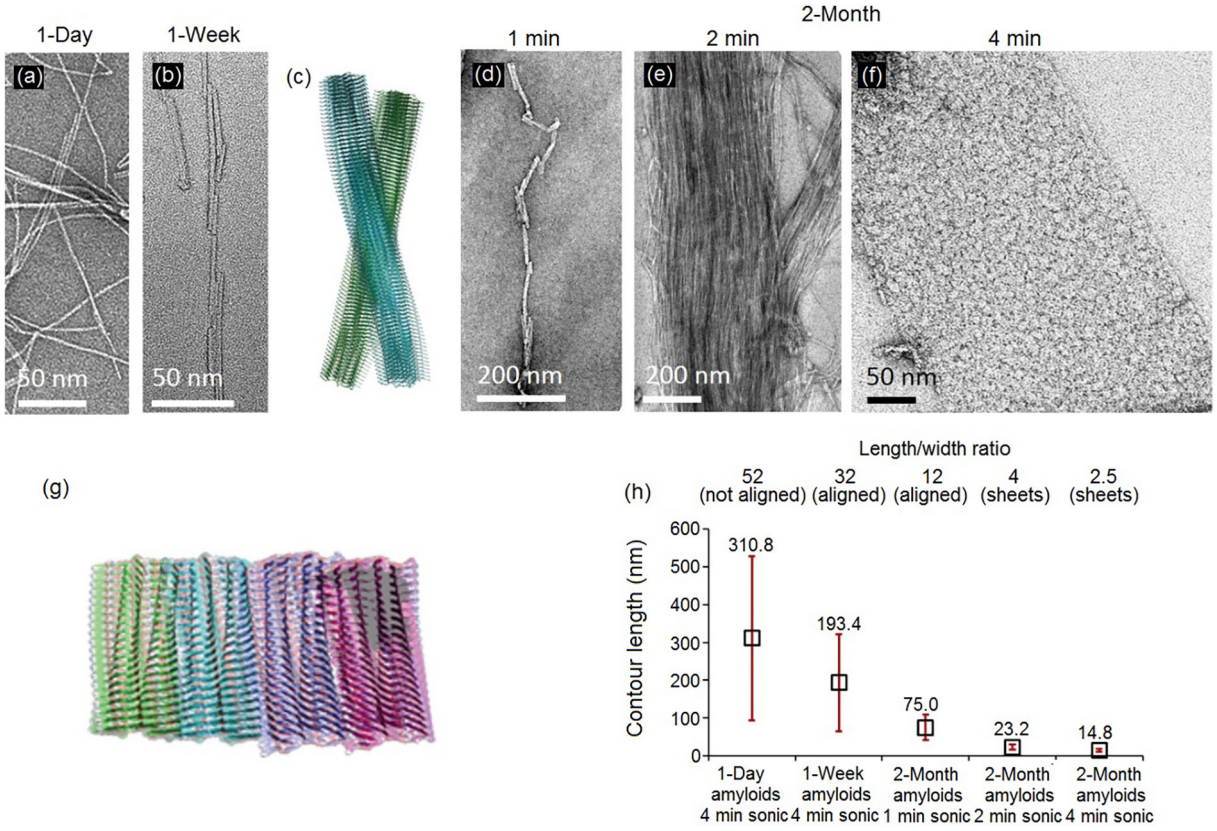

Fig. 3. (Color online) Evolving physical and physicochemical properties of IAPP probed by sonication-induced reassembly. (a) Sonication of 1-day old amyloids was able to break the fibrils into relatively long fragments (>300 nm). (b) Sonication cut 1-week old amyloids into smaller fragments (<200 nm), which re-aligned into "fibrils" after incubation for 18 h. (c) Model structure of two long protofibrils (~37 nm in length with highly twisted lateral surfaces) associated through local lateral interactions, where steric hindrance prevented a maximum lateral alignment of two fibrils. (d)–(f) Depending on sonication energy applied (1, 2 or 4 min), the 2-month aged amyloids broke into very short fragments of different lengths, which were able to re-align into fibrils (e) or form sheet-like structures (f). (g) Model structure of a 2D sheet formed by four short protofibrils (~10 nm in length with a nearly flat lateral surface) with small twists associated laterally. (h) Contour length of sonicated IAPP amyloids. The upper panel represents length to width ratios and assembly behaviors of amyloid fragments after sonication.

like sheets possessed directionality (Fig. 3e), while at *L*/*W* ratio = 2.5 amyloid fragments were seen to assemble into large 2D sheets (Fig. 3f), likely due to the low energy cost of aligning shorter fragments of large quantities.

3.2.3. Self-assembly of IAPP protofibrils, atomistic molecular dynamics simulations

Computer simulations were applied to probe the lateral association of sonicated fragments at the atomic level. Amyloid fibrils have twisted morphologies bundled by multiple protofibrils. Based on solid-state NMR or X-ray microcrystallography studies, U-shaped structural models of protofibrils have been proposed (Fig. S3a online) [28,50], where parallel stacking of the backbones along the fibril axis with a small twist angle forms an elongated protofibril. Our recent high-resolution AFM analysis of IAPP fibrils [48] showed structural polymorphism with most fibrils featuring a ~50 nm crossover periodicity and a small fraction possessing a ~22 nm periodicity. With ~0.5 nm between adjacent peptides along the fibril axis, a protofibril with a 50 nm crossover periodicity features a twist angle of ~1.8° between adjacent peptides (i.e., a 180° rotation for ~100 peptides). Therefore, a short 10 nm protofibril after sonication should have a twist of ~36° with lateral surfaces exposed on one side available for association. The binding energies of two 10 nm IAPP fibril fragments with different inter-protofibril arrangements were estimated (Fig. S3 online). Using the Medusa force field, the binding energies were computed by a Monte Carlo-based sampling of the side chain orientations of all the interface residues [32]. The computational modeling revealed three possible binding modes with lower binding energies (Fig. S3b, c online)—corresponding to *x* and *y* shifts of 1.32 and 4.3 nm for conformation 1, 0.99 and 4.5 nm for conformation 2, and 0.66 and 4.7 nm for conformation 3, respectively. All these binding modes featured close packing of hydrophobic residues exposed on the lateral surfaces of the protofibrils. As a result, short fibril fragments with small twists further self-assembled into 2D sheets as depicted in Fig. 3g, in agreement with the experimental results (e.g., Fig. 3e and f). However, since longer fibrils possessed lateral surfaces not exposed on one side but twisted periodically (Fig. 3c), steric hindrance prevented a maximum lateral alignment of two fibrils, which would otherwise form a large multi-bundled fibril, but rather assumed a non-parallel alignment by burying the lateral hydrophobic surfaces locally.

3.2.4. IAPP aggregation kinetics, through seeding

While the diverse responses of fresh and aged amyloids to ultrasound were indicative of their evolving physical structures, the age of amyloids may impact their toxicity and offer important clues to amyloidosis. Accordingly, we examined the effects of the 2-h, 1-day, 1-week and 2-month old amyloids on the fibrillization kinetics of freshly prepared IAPP (25 μmol/L), at 10:1 (Fig. 4a) and 1:1 (Fig. 4b) of IAPP to seed molar ratios. In both cases, we observed significantly accelerated IAPP fibrillization in the presence of 2-month old amyloids, but only minor effects of the 2-h, 1-day or 1-week old amyloids, likely due to the specific conformational structure of the more aged amyloids which favored secondary nucleation. The lag time of control IAPP was 3 h and the saturation

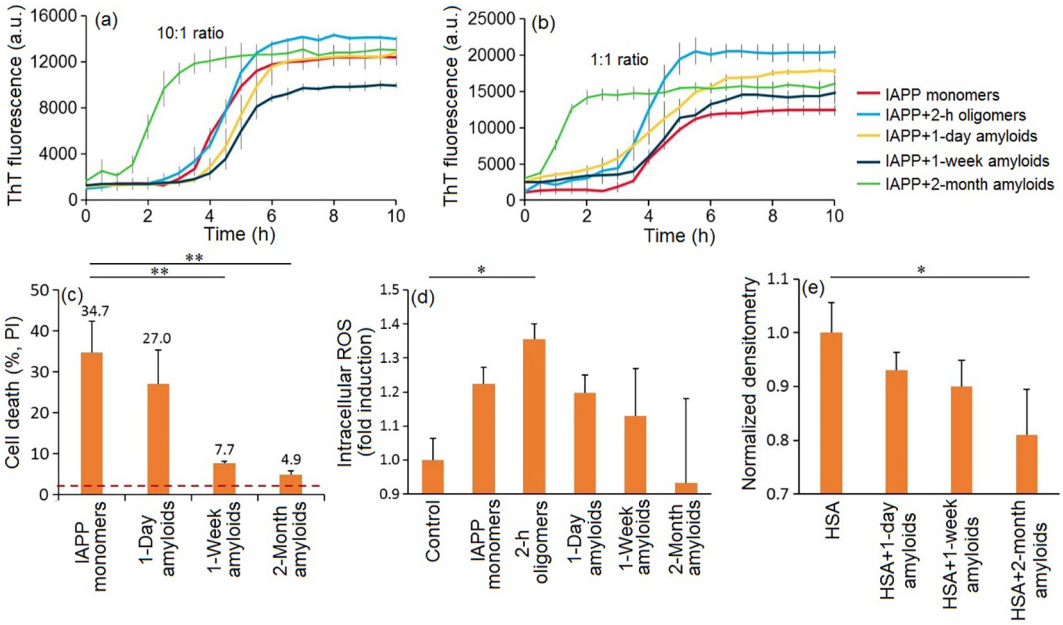

Fig. 4. Kinetics of IAPP fibrillization with seeding and evolving IAPP toxicity in vitro. ThT kinetic assay on IAPP fibrillization (25 μmol/L) in the presence of different amyloid species at 10:1 (a) and 1:1 (b) molar ratios. The lag time of IAPP fibrillization decreased from 3 h for the control to 0.5 h and 1.5 h in the presence of 25 μmol/L (1:1 ratio) and 2.5 μmol/L (10:1 ratio) 2-month old amyloids, whereas no such promotion effect was seen in the presence of 1-day and 1-week old IAPP amyloids. (c) Toxicities of pancreatic βTC6 cells treated with 1-day, 1-week and 2-month old IAPP amyloids, displaying reduced cell death with time. Dashed red line: viability of control untreated cells. (d) DCFH-DA-fluorescence assay of pancreatic βTC6 cells treated with IAPP indicates decreased ROS generation with aging of the fibrils. The 2 h pre-incubated IAPP initiated a higher ROS response than fresh IAPP, due to pre-formed toxic oligomeric species. (e) Quantified band densitometry analysis of blue-native PAGE of 1-day, 1-week and 2-month old IAPP amyloids (100 μmol/L) pre-incubated for 4 h with human serum albumin (HSA; 100 μmol/L) revealed an increased protein binding with aging of the fibrils (original blue-native PAGE gel in Fig. S6 online). *denote statistically significant differences between sample mean to a control mean (ANOVA; $^{*}P \leq 0.05$; $^{**}P \leq 0.01$).

phase was reached within 6 h, whereas 2-month old amyloids shortened IAPP fibrillization lag times down to 1.5 or 0.5 h, at the 10:1 or 1:1 ratio, respectively.

3.3. IAPP amyloid – toxicological properties

3.3.1. IAPP amyloid toxicity in vitro

The 1-day old IAPP amyloids elicited the greatest toxicity among the analyzed mature amyloids (Fig. 4c). Cell death (pancreatic βTC6 beta cells) was determined to be 27.0% ± 8.3%, 7.7% ± 0.4% and 4.9% ± 0.9%, upon treatment with 1-day, 1-week and 2-month old IAPP amyloids, respectively. Similarly, ROS production by different IAPP species decreased with the age of amyloids, whereas fresh and 2-h pre-incubated IAPP (i.e., toxic oligomers) induced most oxidative stress to the cells (Fig. 4d). It has been demonstrated in the literature that fully-matured IAPP, Aβ and α-synuclein fibrils are not the main toxic species and severity of neurodegenerative diseases, such as Alzheimer's [51,52] and Parkinson's diseases [53], often correlates poorly with the extent of amyloid deposition [51], whereas soluble nonfibrillar oligomeric species [54–56] were found to be the major cause for neurodegeneration and toxicity [6,57–64]. On the other hand, our prior statistical analysis [48] revealed that the presence of monomers and oligomers coexisting with the fibrils was minimal by 24 h and decreased further over time, dictated by the aggregation energy landscape of amyloid proteins [65] where the amyloid state is energetically more stable than the oligomeric or monomeric states. Accordingly, the reducing cytotoxicity elicited by IAPP of growing age in the current study may be mainly attributable to the declining population of soluble IAPP species with time. Notably, there are only six residue differences between human and rodent IAPP [66]; however, these changes, particularly in the amyloidogenic region between residues 20–29, are sufficient to render rodent IAPP non-amyloidogenic [67,68] and non-toxic [9].

In addition, the protein binding capacity of IAPP amyloids was elevated with age. Specifically, blue-native PAGE protein band densitometry (Fig. 4e) revealed increased HSA binding to IAPP amyloids, from 7% for 1-day up to 10% and 19% for 1-week and 2-month old fibrils, respectively, indicating increased hydrophobicity and surface roughness over time through continued self-assembly. It is noteworthy that protein corona formation may be an important aspect with regard to the conformation and fate of amyloid proteins in vivo, impacting both fibril formation and the biological identity of mature amyloid fibrils [10,17,69]. For instance, we have recently reported formation of a rapid and largely heterogeneous coating of proteins on the surface of IAPP amyloid fibrils in a complex biological environment [69]. The current finding further illustrates the evolving physicochemical properties of amyloid fibrils, which, in their native environments, would translate to biological and pathological implications.

3.3.2. Toxicity modulation, upon cross seeding of fresh and aged IAPP in vivo

We have recently established and validated an embryonic zebrafish model for examining the aggregation and toxicity of amyloid proteins [70]. The major advantages of this model include the high fecundity and transparency of zebrafish embryos as well as an ultra-small sample volume of nano-liters. To examine the toxicity characteristics of fresh and IAPP in cross-talk, we mixed fresh and different aged IAPP (2-h old oligomers, 1-day, 1-week and 2-month old amyloids) and injected them inside zebrafish embryos 3 h post fertilization (hpf). At this age, zebrafish embryos each displayed approximately 2000 cells on top of the yolk, and the embryos were protected by chorionic membranes. Injecting IAPP peptides, oligomers and amyloids into the perivitelline space of embryos confined their interactions with embryonic cells and any subsequent toxicity was observed in the context of developmental abnormalities or lethal toxicity to zebrafish embryos. First, IAPP ranging from 2 to

50 μmol/L in concentration were injected into zebrafish embryos to determine the LC_{50} value of the peptide. 12 μmol/L of IAPP elicited ~50% toxicity and was therefore selected as the dose for further experiments. Fresh and aged IAPP fibrils were mixed at 1:1 (12 μmol/L each) and 10:1 (12 and 1.2 μmol/L) molar ratios and were subsequently injected inside zebrafish embryos. The 2 h-old IAPP oligomers induced toxicity of ~50% and ~20% at 12 and 1.2 μmol/L, respectively (Fig. 5a and b). Fluorescence imaging with ThT revealed that oligomers directly interacted with the lipid membranes of zebrafish embryonic cells and the embryos were dead by 6 h (Fig. S5a online), whereas mature fibrils did not affect the embryo development up to 12 h (Fig. S5b online). Upon exposure of further aged IAPP, the toxicity was decreased in the order of 1 day > 1 week > 2 months for the fibrils at both concentrations of 12 and 1.2 μmol/L, due to the adsorption and sequestration of toxic oligomers into mature fibrils. Upon mixing fresh IAPP with 2 h-old oligomers at the 1:1 and 10:1 ratios the toxicity was elevated to ~75%, reflecting the combined toxicity of 2 h-old oligomers and oligomers generated from fresh IAPP (Fig. 5a and b). However, when fresh IAPP was mixed with 1-day, 1-week and 2-month old IAPP, their toxicity was slightly enhanced at the 10:1 ratio but suppressed at the 1:1 ratio. This enhanced toxicity at the 10:1 ratio was likely due to the amyloid-assisted IAPP seeding in generating more toxic species, while the decreased toxicity at the 1:1 ratio can be attributed to the much accelerated IAPP fibrillization (i.e., shortened toxic oligomeric phase) that subsequently led to decreased toxicity [71]. It was further explained by ThT assay where enhanced fibrillization and shortened lag phase of fresh IAPP were observed in the presence of aged IAPP amyloids (Fig. 4a and b). ThT imaging in vivo also corroborated that fresh IAPP was sequestered away from embryonic cells (Fig. 5f) by mature fibrils and no ThT fluorescence was observed in the embryonic cells. This is in contrast to the cases of fresh IAPP (Fig. 5d) and oligomers (Fig. 5e), where ThT fluorescence was observed from the cells due to IAPP fibrillization on embryonic membranes.

4. Conclusion

The uncovered structural and toxicity attributes of IAPP amyloids bring forth the notion that amyloid fibrils and plaques evolve both physically and biologically, despite their much reduced and stable energy states [65] compared with native proteins. In addition to IAPP, the current findings may be generally applicable to other classes of amyloid proteins such as Aβ, alpha synuclein and prions, due to their shared characteristics in molecular self-assembly, aggregation, mesoscopic structure and cross-seeding [37,43,72]. Together, this study fills a knowledge gap concerning amyloidosis and points to a dynamic relationship between amyloidosis and aging. The accelerated aggregation, coupled with reduction of IAPP toxicity through seeding and sequestration by aged

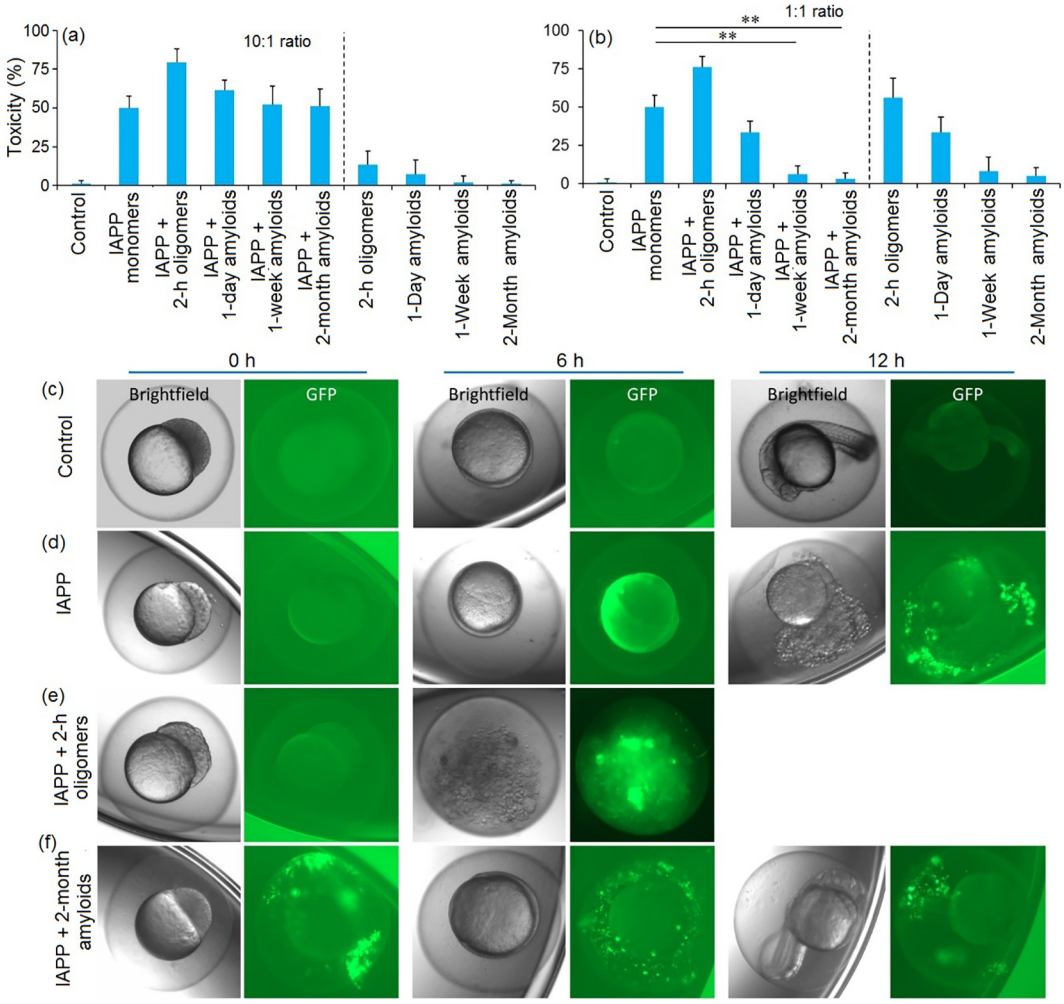

Fig. 5. IAPP toxicity through in vivo seeding. The toxicological impact of cross talk between fresh (12 μmol/L) and different aged IAPP at 10:1 (a) and 1:1 (b) molar ratios. (c)–(f) Brightfield and fluorescence imaging of zebrafish embryo development with injected (d) fresh IAPP, or premixed with (e) 2 h-old oligomeric IAPP or (f) 2-month old amyloids at 1:1 molar ratio after 0, 6 and 12 h. *denote statistically significant differences between sample mean to a control mean (ANOVA; $P \leq 0.05$).

amyloids, alludes to a conspiring role of amyloid fibrils and confounds the perception that the oligomer hypothesis and amyloid hypothesis are mutually exclusive. This, together with the robust capacity of amyloid fibrils and plaques in storing metal ions such as zinc and copper [73–77] that are central to the physiological cellular function and native stabilization of amyloid proteins, highlights long-term biological implications of amyloid proteins, amyloid fibrils and plaques. Furthermore, amyloid proteins in the intra- (e.g., tau and alpha synuclein) or extra-cellular space (e.g., IAPP and Aβ) can not only self-assemble but also interact with proteins, cellular membranes and other organelles to compromise their function, through hydrophobic and electrostatic interactions, hydrogen bonding, as well as ROS production [1–4]. Exploiting such interactions may advance our understanding of cell degeneration and aid in the design of effective mitigation strategies against amyloid diseases, a field eagerly awaits breakthroughs despite decades of research and investments [78].

Conflict of interest

The authors declare that they have no conflict of interest.

Acknowledgments

This work was supported by ARC Project CE140100036 (Davis), NSF CAREER CBET-1553945 (Ding), NIH MIRA R35GM119691 (Ding) and Monash Institute of Pharmaceutical Sciences (Ke). Davis is thankful for the award of an ARC Australian Laureate Fellowship. Purcell is supported by a Principal Research Fellowship from the Australian NHMRC. Pilkington acknowledges an Australian Government Research Training Program (RTP) Scholarship. Javed acknowledges Monash International Postgraduate Research Scholarship. Javed and Lin thank Shanghai Science and Technology Commission "Belt and Road" Initiative Program (17230743000).

Appendix A. Supplementary material

Supplementary data to this article can be found online at https://doi.org/10.1016/j.scib.2018.11.012.

References

[1] Knowles TPJ, Vendruscolo M, Dobson CM. The amyloid state and its association with protein misfolding diseases. Nat Rev Mol Cell Biol 2014;15:384–96.
[2] Eisenberg D, Jucker M. The amyloid state of proteins in human diseases. Cell 2012;148:1188–203.
[3] Sawaya MR, Sambashivan S, Nelson R, et al. Atomic structures of amyloid cross-[bgr] spines reveal varied steric zippers. Nature 2007;447:453–7.
[4] Ke PC, Sani MA, Ding F, et al. Implications of peptide assemblies in amyloid diseases. Chem Soc Rev 2017;46:6492–531.
[5] Zraika S, Hull RL, Verchere CB, et al. Toxic oligomers and islet beta cell death: guilty by association or convicted by circumstantial evidence? Diabetologia 2010;53:1046–56.
[6] Haataja L, Gurlo T, Huang CJ, et al. Islet amyloid in type 2 diabetes, and the toxic oligomer hypothesis. Endocr Rev 2008;29:303–16.
[7] Nedumpully-Govindan P, Kakinen A, Pilkington EH, et al. Stabilizing off-pathway oligomers by polyphenol nanoassemblies for iapp aggregation inhibition. Sci Rep 2016;6:19463.
[8] Hardy J, Higgins G. Alzheimer's disease: the amyloid cascade hypothesis. Science 1992;256:184–5.
[9] Krotee P, Rodriguez JA, Sawaya MR, et al. Atomic structures of fibrillar segments of hiapp suggest tightly mated β-sheets are important for cytotoxicity. eLife 2017;6:e19273.
[10] Pilkington EH, Gurzov EN, Kakinen A, et al. Pancreatic β-cell membrane fluidity and toxicity induced by human islet amyloid polypeptide species. Sci Rep 2016;6:21274.
[11] Meyer-Luehmann M, Coomaraswamy J, Bolmont T, et al. Exogenous induction of cerebral ß-amyloidogenesis is governed by agent and host. Science 2006;313:1781–4.
[12] Langer F, Eisele YS, Fritschi SK, et al. Soluble Aβ seeds are potent inducers of cerebral β-amyloid deposition. J Neurosci 2011;31:14488–95.
[13] Stöhr J, Watts JC, Mensinger ZL, et al. Purified and synthetic alzheimer's amyloid beta (aβ) prions. Proc Natl Acad Sci USA 2012;109:11025–30.
[14] Lu JX, Qiang W, Yau WM, et al. Molecular structure of β-amyloid fibrils in alzheimer's disease brain tissue. Cell 2013;154:1257–68.
[15] Petkova AT, Leapman RD, Guo Z, et al. Self-propagating, molecular-level polymorphism in alzheimer's β-amyloid fibrils. Science 2005;307:262–5.
[16] Tycko R. Physical and structural basis for polymorphism in amyloid fibrils. Protein Sci 2014;23:1528–39.
[17] Pilkington EH, Xing Y, Wang B, et al. Effects of protein corona on IAPP amyloid aggregation, fibril remodelling, and cytotoxicity. Sci Rep 2017;7:2455.
[18] Salamekh S, Brender JR, Hyung SJ, et al. A two-site mechanism for the inhibition of iapp amyloidogenesis by zinc. J Mol Biol 2011;410:294–306.
[19] Brender JR, Hartman K, Nanga RPR, et al. Role of zinc in human islet amyloid polypeptide aggregation. J Am Chem Soc 2010;132:8973–83.
[20] Bellia F, Grasso G. The role of copper(II) and zinc(II) in the degradation of human and murine iapp by insulin-degrading enzyme. J Mass Spectrom 2014;49:274–9.
[21] Ge X, Kakinen A, Gurzov EN, et al. Zinc-coordination and c-peptide complexation: a potential mechanism for the endogenous inhibition of iapp aggregation. Chem Commun 2017;53:9394–7.
[22] Cao P, Abedini A, Wang H, et al. Islet amyloid polypeptide toxicity and membrane interactions. Proc Natl Acad Sci USA 2013;110:19279–84.
[23] Sparr E, Engel MFM, Sakharov DV, et al. Islet amyloid polypeptide-induced membrane leakage involves uptake of lipids by forming amyloid fibers. FEBS Lett 2004;577:117–20.
[24] Mathiason CK. Silent prions and covert prion transmission. PLoS Pathog 2015;11:e1005249.
[25] Schindelin J, Arganda-Carreras I, Frise E, et al. Fiji: an open-source platform for biological-image analysis. Nat Methods 2012;9:676.
[26] Lin S, Zhao Y, Xia T, et al. High content screening in zebrafish speeds up hazard ranking of transition metal oxide nanoparticles. ACS Nano 2011;5:7284–95.
[27] Usov I, Mezzenga R. Fiberapp: an open-source software for tracking and analyzing polymers, filaments, biomacromolecules, and fibrous objects. Macromolecules 2015;48:1269–80.
[28] Luca S, Yau WM, Leapman R, et al. Peptide conformation and supramolecular organization in amylin fibrils: constraints from solid state nmr. Biochemistry 2007;46:13505–22.
[29] Ding F, Yin S, Dokholyan NV. Rapid flexible docking using a stochastic rotamer library of ligands. J Chem Inf Model 2010;50:1623–32.
[30] Yin S, Ding F, Dokholyan NV. Eris: an automated estimator of protein stability. Nat Methods 2007;4:466.
[31] Yin S, Ding F, Dokholyan NV. Modeling backbone flexibility improves protein stability estimation. Structure 2007;15:1567–76.
[32] Ding F, Dokholyan NV. Emergence of protein fold families through rational design. PLOS Comput Biol 2006;2:e85.
[33] Nedumpully-Govindan P, Jemec DB, Ding F. Csar benchmark of flexible medusadock in affinity prediction and nativelike binding pose selection. J Chem Inf Model 2016;56:1042–52.
[34] Sarroukh R, Cerf E, Derclaye S, et al. Transformation of amyloid β(1–40) oligomers into fibrils is characterized by a major change in secondary structure. Cell Mol Life Sci 2011;68:1429–38.
[35] Kahle PJ, Neumann M, Ozmen L, et al. Selective insolubility of α-synuclein in human lewy body diseases is recapitulated in a transgenic mouse model. Am J Pathol 2001;159:2215–25.
[36] Lashuel HA, Petre BM, Wall J, et al. A-synuclein, especially the parkinson's disease-associated mutants, forms pore-like annular and tubular protofibrils. J Mol Biol 2002;322:1089–102.
[37] Tsigelny IF, Crews L, Desplats P, et al. Mechanisms of hybrid oligomer formation in the pathogenesis of combined alzheimer's and parkinson's diseases. PLoS One 2008;3:e3135.
[38] van Diggelen F, Tepper AWJW, Apetri MM, et al. A-synuclein oligomers: a study in diversity. Isr J Chem 2017;57:1–26.
[39] Adamcik J, Lara C, Usov I, et al. Measurement of intrinsic properties of amyloid fibrils by the peak force qnm method. Nanoscale 2012;4:4426–9.
[40] Ohhashi Y, Kihara M, Naiki H, et al. Ultrasonication-induced amyloid fibril formation of β2-microglobulin. J Biol Chem 2005;280:32843–8.
[41] Chatani E, Lee YH, Yagi H, et al. Ultrasonication-dependent production and breakdown lead to minimum-sized amyloid fibrils. Proc Natl Acad Sci USA 2009;106:11119–24.
[42] Hu X, Crick SL, Bu G, et al. Amyloid seeds formed by cellular uptake, concentration, and aggregation of the amyloid-beta peptide. Proc Natl Acad Sci USA 2009;106:20324–9.
[43] Horvath I, Wittung-Stafshede P. Cross-talk between amyloidogenic proteins in type-2 diabetes and parkinson's disease. Proc Natl Acad Sci USA 2016;113:12473–7.
[44] Xu F, Fu Z, Dass S, et al. Cerebral vascular amyloid seeds drive amyloid β-protein fibril assembly with a distinct anti-parallel structure. Nat Commun 2016;7:13527.
[45] Leinenga G, Götz J. Scanning ultrasound removes amyloid-β and restores memory in an alzheimer's disease mouse model. Sci Transl Med 2015;7:278ra233.
[46] Taurozzi J, Hackely V, Wiesner M. A standardised approach for the dispersion of titanium dioxide nanoparticles in biological media. Nanotoxicology 2013;7:389–401.
[47] Kakinen A, Kahru A, Nurmsoo H, et al. Solubility-driven toxicity of CuO nanoparticles to $Caco_2$ cells and *Escherichia coli*: effect of sonication energy and test environment. Toxicol Vitro 2016;36:172–9.

[48] Kakinen A, Adamcik J, Wang B, et al. Nanoscale inhibition of polymorphic and ambidextrous iapp amyloid aggregation with small molecules. Nano Res 2018;11:3636–47.
[49] Adamcik J, Sánchez-Ferrer A, Ait-Bouziad N, et al. Microtubule-binding R3 fragment from tau self-assembles into giant multistranded amyloid ribbons. Angew Chem Int Ed 2016;55:618–22.
[50] Wiltzius JJW, Sievers SA, Sawaya MR, et al. Atomic structure of the cross-β spine of islet amyloid polypeptide (amylin). Protein Sci 2008;17:1467–74.
[51] Hardy J, Selkoe DJ. The amyloid hypothesis of alzheimer's disease: progress and problems on the road to therapeutics. Science 2002;297:353–6.
[52] Tanzi RE, Bertram L. Twenty years of the alzheimer's disease amyloid hypothesis: a genetic perspective. Cell 2005;120:545–55.
[53] Ryu EJ, Harding HP, Angelastro JM, et al. Endoplasmic reticulum stress and the unfolded protein response in cellular models of parkinson's disease. J Neurosci 2002;22:10690–8.
[54] Nanga RPR, Brender JR, Vivekanandan S, et al. Structure and membrane orientation of iapp in its natively amidated form at physiological ph in a membrane environment. Biochim Biophys Acta, Biomembr 2011;1808: 2337–42.
[55] Pham JD, Chim N, Goulding CW, et al. Structures of oligomers of a peptide from β-amyloid. J Am Chem Soc 2013;135:12460–7.
[56] Rodriguez JA, Ivanova MI, Sawaya MR, et al. Structure of the toxic core of α-synuclein from invisible crystals. Nature 2015;525:486.
[57] Janson J, Ashley RH, Harrison D, et al. The mechanism of islet amyloid polypeptide toxicity is membrane disruption by intermediate-sized toxic amyloid particles. Diabetes 1999;48:491–8.
[58] Mirzabekov TA, Lin M, Kagan BL. Pore formation by the cytotoxic islet amyloid peptide amylin. J Biol Chem 1996;271:1988–92.
[59] Nimmrich V, Grimm C, Draguhn A, et al. Amyloid β oligomers (Aβ1–42 globulomer) suppress spontaneous synaptic activity by inhibition of p/q-type calcium currents. J Neurosci 2008;28:788–97.
[60] Shankar GM, Li S, Mehta TH, et al. Amyloid-β protein dimers isolated directly from alzheimer's brains impair synaptic plasticity and memory. Nat Med 2008;14:837.
[61] Zhang Y, Lu L, Jia J, et al. A lifespan observation of a novel mouse model: *In vivo* evidence supports aβ oligomer hypothesis. PLoS One 2014;9:e85885.
[62] Pham E, Crews L, Ubhi K, et al. Progressive accumulation of amyloid-β oligomers in Alzheimer's disease and in amyloid precursor protein transgenic mice is accompanied by selective alterations in synaptic scaffold proteins. FEBS J 2010;277:3051–67.
[63] Giasson BI, Duda JE, Quinn SM, et al. Neuronal a-synucleinopathy with severe movement disorder in mice expressing A53t human a-synuclein. Neuron 2002;34:521–33.
[64] Winner B, Jappelli R, Maji SK, et al. In vivo demonstration that α-synuclein oligomers are toxic. Proc Natl Acad Sci USA 2011;108:4194–9.
[65] Adamcik J, Mezzenga R. Amyloid polymorphism in the protein folding and aggregation energy landscape. Angew Chem Int Ed 2018;57:8370–82.
[66] Rulifson IC, Cao P, Miao L, et al. Identification of human islet amyloid polypeptide as a BACE2 substrate. PLoS One 2016;11:e0147254.
[67] Goldsbury C, Goldie K, Pellaud J, et al. Amyloid fibril formation from full-length and fragments of amylin. J Struct Biol 2000;130:352–62.
[68] Westermark P, Engström U, Johnson KH, et al. Islet amyloid polypeptide: pinpointing amino acid residues linked to amyloid fibril formation. Proc Natl Acad Sci USA 1990;87:5036–40.
[69] Pilkington EH, Gustafsson OJR, Xing Y, et al. Profiling the serum protein corona of fibrillar human islet amyloid polypeptide. ACS Nano 2018;12:6066–78.
[70] Javed I, Yu T, Peng G, et al. In vivo mitigation of amyloidogenesis through functional-pathogenic double protein coronae. Nano Lett 2018;18:5797–804.
[71] Pilkington EH, Lai M, Ge X, et al. Star polymers reduce islet amyloid polypeptide toxicity via accelerated amyloid aggregation. Biomacromolecules 2017;18:4249–60.
[72] Yoon G, Lee M, Kim JI, et al. Role of sequence and structural polymorphism on the mechanical properties of amyloid fibrils. PLoS One 2014;9:e88502.
[73] Lovell MA, Robertson JD, Teesdale WJ, et al. Copper, iron and zinc in alzheimer's disease senile plaques. J Neurol Sci 1998;158:47–52.
[74] Hayne DJ, Lim S, Donnelly PS. Metal complexes designed to bind to amyloid-α for the diagnosis and treatment of alzheimer's disease. Chem Soc Rev 2014;43:6701–15.
[75] Lee M, Wang T, Makhlynets OV, et al. Zinc-binding structure of a catalytic amyloid from solid-state nmr. Proc Natl Acad Sci USA 2017;114:6191–6.
[76] Al-Garawi ZS, McIntosh BA, Neill-Hall D, et al. The amyloid architecture provides a scaffold for enzyme-like catalysts. Nanoscale 2017;9:10773–83.
[77] Geng J, Li M, Wu L, et al. Liberation of copper from amyloid plaques: making a risk factor useful for alzheimer's disease treatment. J Med Chem 2012;55:9146–55.
[78] Lancet T. Alzheimer's disease: expedition into the unknown. Lancet 2016;388:2713.

Aleksandr Kakinen is a Postdoctoral Research Fellow at CBNS, Monash University, Australia. While working at the National Institute of Chemical Physics and Biophysics, Tallinn, Estonia, he obtained his Ph.D. degree (2014) at Tallinn University of Technology, Estonia. His research interests include amyloidogenesis, type 2 diabetes, dementia, protein corona, nano- and ecotoxicology.

Pu Chun Ke is a Signature Project Leader at CBNS, Monash University. He was a Distinguished Visiting Scientist at CSIRO, Australia (2014) and tenured Associate Professor (2009–2013) and Assistant Professor (2003–2009) at Clemson University, USA, after his postdoctoral research at the University of California, San Diego. His current research is focused on amyloid diseases, protein aggregation, protein corona and nanotoxicology.

Thomas Davis is an Australian Laureate Fellow, Fellow of the Australian Academy of Science, and Director of CBNS at Monash University. Prior to his appointment at Monash he spent 21 years as a senior academic at the University of New South Wales in Sydney. His research focuses on the applications of polymer science and nanotechnology for medicine and biotechnology.